Low-energy excitonic condensate excitations in semimetal and semiconducting materials

Thi-Hong-Hai Do [1], Minh-Tien Tran [2] and Van-Nham Phan [3,4,*]

[1] *Department of Physics, Hanoi University of Mining and Geology, Duc Thang, Bac Tu Liem, Hanoi, Vietnam*
[2] *Institute of Physics, Vietnam Academy of Science and Technology, Cau Giay, Hanoi, Vietnam*
[3] *Institute of Research and Development, Duy Tan University, 3 Quang Trung, Da Nang, Vietnam*
[4] *Faculty of Natural Sciences, Duy Tan University, 3 Quang Trung, Da Nang, Vietnam*

(Received 23 March 2022; revised 24 May 2022; accepted 5 July 2022; published 13 July 2022)

The low-energy excitation properties of the excitonic condensate in the semimetal and semiconducting materials are inspected in the extended Falicov-Kimball model. In the framework of the unrestricted Hartree-Fock approximation, we have released a set of self-consistent equations so the excitonic condensate order parameter and then the optical conductivity and the dynamical excitonic susceptibility function are evaluated. We find that the optical conductivity becomes significant and shows a sharp peak at a frequency that is twice as of the excitonic condensate order parameter once the system settles in the excitonic condensate. In the meanwhile, out of the excitonic condensation state, the dynamical excitonic susceptibility function in the semimetal state releases a dominant peak at low frequency if Coulomb interaction is sufficiently large. This character indicates the possibility of the resonance bound excitonic condensate even in high-temperature normal semimetals. The resonance is dramatically reinforced inside of the semiconducting state and that specifies the stability of the bound excitonic coherent state of the preformed excitons in the semiconducting materials.

DOI: 10.1103/PhysRevB.106.035120

I. INTRODUCTION

The macroscopic coherent state of excitons–bosonic quasiparticles composited by electrons and holes owing to the Coulomb interaction is always one of the most important issues attracting much interest in research in condensed-matter physics. Proposed theoretically more than 60 years ago [1–3], the nature of the condensation state of excitons possibly stabilizes in semimetals or semiconductors up to now is still in debate. It has been widely understood that, in a semimetal, the formation and condensate of excitons might establish simultaneously and be described by the Bardeen-Cooper-Schrieffer (BCS) theory similar to the superconducting state, whereas, in semiconductors, the excitonic condensate can be viewed as the Bose-Einstein condensation (BEC) of preformed excitons like neutral atoms [4,5]. However, recent optical conductivity measurements have revealed that the excitons in quasi-one-dimensional (1D) semimetal Ta_2NiSe_5 can be formed before condensing even in the semimetal phase [6,7]. The observation has promoted investigating the dynamical signatures of the excitonic condensate [8–12], which is an essential point help us clear the nature of the excitonic condensation fluctuations both above and below the critical point of the condensation state.

To analyze theoretically the formation and condensation of excitons in semimetal and semiconducting materials, a two-band model describing the electron-hole system is usually applicable [1–4]. In that model, the Coulomb interaction between electrons and holes is included, which induces the electron-hole hybridization, the coherent state of excitons then might be established. One of the most typical two-band models is an extended Falicov-Kimball model (EFKM) that is the extension of the original Falicov-Kimball model once the valence band is dispersed [5]. Using the EFKM, the excitonic condensation state in semimetal-semiconducting transition materials has been intensively investigated [5,13–15]. However, in these studies, the dynamical properties of the excitonic condensation state have not been examined. In the meanwhile, analyzing dynamical signatures both inside and outside of an ordered state is a crucial point in understanding the fluctuations of the coherent states and help us clear the nature of the order state [6–9,11,12,16]. Indeed, analyzing the optical conductivity spectra has revealed the anomalous appearance of the excitons even before the excitonic condensation in metallic Ta_2NiSe_5 [6,7]. The preformed excitons are also found in the semiconductor side, the so-called "halo" of the excitonic condensate by inspecting the dynamical excitonic susceptibility in the EFKM [16] that has been experimentally observed in the semiconductor side of the two-dimensional (2D) semimetal-semiconductor transition compound $TmSe_{0.45}Te_{0.55}$ [17,18]. Or most recently, by measuring the Raman conductivity, one has revealed the anomalous excitonic fluctuations in Ta_2NiSe_5 whose intensity grows inversely with temperature toward the Weiss temperature [9].

In experiments, dynamical properties in a condensed state can be inspected in angle-resolved photoemission spectroscopy measurements. However, due to the limitation of the measurement to occupied states below the Fermi level, the formation of an excitation gap below a critical temperature has not been unveiled. In the present paper, we

*Corresponding author: phanvannham@duytan.edu.vn

investigate the dynamical properties of the excitonic condensation state in theoretically in signatures of the optical conductivity and dynamical excitonic susceptibility function. The former provides insight into the excitonic condensation state in the systems, whereas, the latter emerges the electron-hole coherent fluctuations before the stability of the excitonic condensation state. In the framework of the unrestricted Hartree-Fock (UHF) approximation, the optical conductivity has been addressed in the EFKM under the influence of the mass imbalance [10]. The optical conductivity in the EFKM and the dynamical excitonic susceptibility in a similar EFKM the so-called two-orbital Hubbard model have been also investigated by using respectively the dynamical density matrix renormalization group method [6] and the dynamical mean-field theory [11,12]. However, these studies are limited to the weak coupling and low-temperature regime. That obviously could not consider the halo phase and also high-temperature excitonic fluctuations in the situation of strong Coulomb interaction.

In the present paper, the optical conductivity and the dynamical excitonic susceptibility function are addressed in the framework of the EFKM. By using the UHF approximation, we find a set of self-consistent equations so the excitonic order parameters and quasiparticle energies once the hybridization between electron and hole driven by the Coulomb interaction in the EFKM are resolved. That helps us evaluate explicitly the optical conductivity in the features of Kubo linear response theory and the dynamical excitonic susceptibility function in the random phase approximation. The numerical results thus might reveal in detail the low-energy dynamical features of the excitonic condensation state both below and above the excitonic condensate points. We agree generally that the UHF approximation is reliable for small interactions, however, it might be also applicable even for large interacting cases in some specific conditions. For instance, in the case of the high-temperature with short or finite range interactions, the correlation length ξ tends to zero as $\xi \sim T^{-1/2}$ [19]. The correlations in the systems thus become less important in case of large temperature. That is synonymous with a weak-coupling situation and reasonably the UHF approximation is applicable in a range of large temperature whatever the interaction is weak or strong [20–22]. In our study, the dynamical excitonic susceptibility function in the EFKM is examined at a very large temperature and we believe that the UHF approximation is reliable also for large Coulomb interaction.

This article is organized as follows. In Sec. II, we introduce the EFKM and its solutions in the UHF approximation. The analytical evaluations for the dynamical quantities such as the optical conductivity and the dynamical excitonic susceptibility function are presented briefly in Sec. III. Section IV shows the numerical results and discussions. The conclusions of the paper can be found in the final section.

II. HAMILTONIAN AND METHOD

In order to inspect the dynamical excitonic excitations, we start with a consideration of the Hamiltonian that describes the electron-hole system possibly forming excitons. The appropriated Hamiltonian of the electron-hole system in the tight-binding approximation might be written as follows:

$$\mathcal{H} = -t^a \sum_{\langle i,j\rangle} a_i^\dagger a_j - t^b \sum_{\langle i,j\rangle} b_i^\dagger b_j + U \sum_i n_i^a n_i^b + (\varepsilon^a - \mu) \sum_i n_i^a + (\varepsilon^b - \mu) \sum_i n_i^b, \quad (1)$$

where $a_i^{(\dagger)}$ and $b_i^{(\dagger)}$ are respectively the spinless fermionic annihilation (creation) operators of the conduction and valence electrons at lattice site i. $t^{a(b)}$ is the nearest-neighbor hopping integral of the conduction (valence) electrons. The first two terms thus describe the kinetic energy of the electron-hole system. The third term addresses the local Coulomb interaction between the conduction and valence electrons with respect to the occupation operators $n_i^a = a_i^\dagger a_i$ and $n_i^b = b_i^\dagger b_i$. $\varepsilon^{a(b)}$ and μ are on-site energy of the conduction (valence) electron and chemical potential. In case $t^b = 0$, i.e., all valence electrons are localized, the Hamiltonian written in Eq. (1) recovers the original Falicov-Kimball model [23], on the other hand, with $t^a = t^b$ it is the single band Hubbard model [24]. In a general case, $t^b \neq 0$, the Hamiltonian in Eq. (1), the so-called extended Falicov-Kimball model has been intensively adapted to analyze the excitonic condensation state in the semimetal-semiconductor transition materials [5,10,13,15,25]. Using the Fourier transformation, for instance, $a_i^\dagger = \frac{1}{\sqrt{N}} \sum_{\mathbf{k}} e^{i\mathbf{R}_i\mathbf{k}} a_{\mathbf{k}}^\dagger$, the Hamiltonian in Eq. (1) can be rewritten in the momentum space, likely as

$$\mathcal{H} = \sum_{\mathbf{k}} (\varepsilon_{\mathbf{k}}^a a_{\mathbf{k}}^\dagger a_{\mathbf{k}} + \varepsilon_{\mathbf{k}}^b b_{\mathbf{k}}^\dagger b_{\mathbf{k}}) + \frac{U}{N} \sum_{\mathbf{k}\mathbf{k}'\mathbf{q}} b_{\mathbf{k}+\mathbf{q}}^\dagger b_{\mathbf{k}'} a_{\mathbf{k}'-\mathbf{q}}^\dagger a_{\mathbf{k}}, \quad (2)$$

where N is the number of lattice sites, and

$$\varepsilon_{\mathbf{k}}^{a(b)} = \varepsilon^{a(b)} - 2t^{a(b)}(\cos k_x + \cos k_y) - \mu, \quad (3)$$

are the electronic dispersion of conduction (valence) electrons in a 2D hypercubic lattice. Here, we have written the Hamiltonian in 2D momentum space. That is applicable to describe the excitonic states in the 2D semimetal-semiconductor transition compound $TmSe_{0.45}Te_{0.55}$ or quasi-1D semimetal Ta_2NiSe_5.

Because of the many-body features, the Hamiltonian in Eq. (1) is impossible to be solved exactly. In the present paper, we use the unrestricted Hartree-Fock approximation by leaving out all fluctuation parts, the effective Hamiltonian then is written as

$$\mathcal{H}_{\text{eff}} = \sum_{\mathbf{k}} (\bar{\varepsilon}_{\mathbf{k}}^a a_{\mathbf{k}}^\dagger a_{\mathbf{k}} + \bar{\varepsilon}_{\mathbf{k}}^b b_{\mathbf{k}}^\dagger b_{\mathbf{k}}) + \delta \sum_{\mathbf{k}} (b_{\mathbf{k}}^\dagger a_{\mathbf{k}} + a_{\mathbf{k}}^\dagger b_{\mathbf{k}}). \quad (4)$$

Here the electronic excitation energies have been replaced with the contribution of the Coulomb interaction given by

$$\bar{\varepsilon}_{\mathbf{k}}^{a(b)} = \varepsilon_{\mathbf{k}}^{a(b)} + U n^{b(a)}, \quad (5)$$

where $n^a = \sum_{\mathbf{k}} \langle a_{\mathbf{k}}^\dagger a_{\mathbf{k}} \rangle / N$ and $n^b = \sum_{\mathbf{k}} \langle b_{\mathbf{k}}^\dagger b_{\mathbf{k}} \rangle / N$, respectively, are the conduction and valence electronic densities evaluated in the momentum space. δ in the effective Hamiltonian denotes for

$$\delta = -\frac{U}{N} \sum_{\mathbf{k}} \langle a_{\mathbf{q}}^\dagger b_{\mathbf{q}} \rangle, \quad (6)$$

which plays the role of the excitonic condensate order parameter, addressing a hybridization of the conduction and valence

electrons, leading to the formation and a condensation of excitons in the system.

The effective Hamiltonian in Eq. (4) might be diagonalized by using the Bogoliubov transformation by defining new fermionic operators

$$\bar{a}_{\mathbf{k}}^{\dagger} = \xi_{\mathbf{k}} b_{\mathbf{k}}^{\dagger} + \eta_{\mathbf{k}} a_{\mathbf{k}}^{\dagger}, \tag{7}$$

$$\bar{b}_{\mathbf{k}}^{\dagger} = -\eta_{\mathbf{k}} b_{\mathbf{k}}^{\dagger} + \xi_{\mathbf{k}} a_{\mathbf{k}}^{\dagger}, \tag{8}$$

where $\xi_{\mathbf{k}}$ and $\eta_{\mathbf{k}}$ are chosen such that $\xi_{\mathbf{k}}^2 + \eta_{\mathbf{k}}^2 = 1$, then one finds

$$\xi_{\mathbf{k}}^2 = \frac{1}{2}\left[1 + \mathrm{sgn}\left(\bar{\varepsilon}_{\mathbf{k}}^{a} - \bar{\varepsilon}_{\mathbf{k}}^{b}\right)\frac{\bar{\varepsilon}_{\mathbf{k}}^{a} - \bar{\varepsilon}_{\mathbf{k}}^{b}}{\Gamma_{\mathbf{k}}}\right],$$
$$\eta_{\mathbf{k}}^2 = \frac{1}{2}\left[1 - \mathrm{sgn}\left(\bar{\varepsilon}_{\mathbf{k}}^{a} - \bar{\varepsilon}_{\mathbf{k}}^{b}\right)\frac{\bar{\varepsilon}_{\mathbf{k}}^{a} - \bar{\varepsilon}_{\mathbf{k}}^{b}}{\Gamma_{\mathbf{k}}}\right], \tag{9}$$

with

$$\Gamma_{\mathbf{k}} = \sqrt{\left(\bar{\varepsilon}_{\mathbf{k}}^{b} - \bar{\varepsilon}_{\mathbf{k}}^{a}\right)^2 + 4|\delta|^2}. \tag{10}$$

In the new fermionic operator representation, the effective Hamiltonian in Eq. (4) can be rewritten in a diagonal form as

$$\mathcal{H}_{\mathrm{dia}} = \sum_{\mathbf{k}} (E_{\mathbf{k}}^{a} \bar{a}_{\mathbf{k}}^{\dagger} \bar{a}_{\mathbf{k}} + E_{\mathbf{k}}^{b} \bar{b}_{\mathbf{k}}^{\dagger} \bar{b}_{\mathbf{k}}), \tag{11}$$

with the respective quasiparticle energies

$$E_{\mathbf{k}}^{a/b} = \frac{\bar{\varepsilon}_{\mathbf{k}}^{a} + \bar{\varepsilon}_{\mathbf{k}+q}^{b}}{2} \mp \frac{\mathrm{sgn}\left(\bar{\varepsilon}_{\mathbf{k}}^{a} - \bar{\varepsilon}_{\mathbf{k}+q}^{b}\right)}{2}\Gamma_{\mathbf{k}}. \tag{12}$$

In the diagonal form of Eq. (11), one easily evaluates the expectation values such that

$$\langle n_{\mathbf{k}}^{a} \rangle = \langle a_{\mathbf{k}}^{\dagger} a_{\mathbf{k}} \rangle = \eta_{\mathbf{k}}^2 n_F\left(E_{\mathbf{k}}^{a}\right) + \xi_{\mathbf{k}}^2 n_F\left(E_{\mathbf{k}}^{b}\right),$$
$$\langle n_{\mathbf{k}}^{b} \rangle = \langle b_{\mathbf{k}}^{\dagger} b_{\mathbf{k}} \rangle = \xi_{\mathbf{k}}^2 n_F\left(E_{\mathbf{k}}^{a}\right) + \eta_{\mathbf{k}}^2 n_F\left(E_{\mathbf{k}}^{b}\right), \tag{13}$$
$$\langle \delta_{\mathbf{k}} \rangle = \langle a_{\mathbf{q}}^{\dagger} b_{\mathbf{q}} \rangle = \left[n_F\left(E_{\mathbf{k}}^{b}\right) - n_F\left(E_{\mathbf{k}}^{a}\right)\right]\mathrm{sgn}\left(\bar{\varepsilon}_{\mathbf{k}}^{a} - \bar{\varepsilon}_{\mathbf{k}}^{b}\right)\frac{\delta}{\Gamma_{\mathbf{k}}},$$

where $n_F(E_{\mathbf{k}})$ denotes for the Fermi distribution function, given by

$$n_F(E_{\mathbf{k}}) = \frac{1}{1 + e^{\beta E_{\mathbf{k}}}}, \tag{14}$$

with $\beta = 1/T$ and T is the temperature.

From Eqs. (5), (6), and (13) one finds a set of self-consistent equations, so the excitonic condensate order parameters and quasi-particle energies can be evaluated by several numerical calculation routines. These results might help us evaluate some dynamical quantities addressed in the following sections.

III. DYNAMICAL QUANTITIES

A. Optical conductivity

To discuss the dynamical properties of the excitonic condensate in the system addressed in the Hamiltonian equation (1), firstly we consider the optical absorption spectrum by analyzing the optical conductivity. In the linear response theory, the optical conductivity can be inspected by using the Kubo formula [26], given by

$$\sigma(\omega) = \frac{i}{\omega}\frac{1}{N^2}\sum_{\mathbf{k}\mathbf{k}'} \langle\langle \mathbf{j}^{\dagger}(\mathbf{k}) | \mathbf{j}(\mathbf{k}') \rangle\rangle_{\mathcal{H}}. \tag{15}$$

Here $\langle\langle \ldots \rangle\rangle_{\mathcal{H}}$ denotes the two-particle retarded correlation function with respect to a Hamiltonian $\mathcal{H}$ and $\mathbf{j}(\mathbf{k})$ is the momentum dependence of the current operator. For the electron-hole system described by the Hamiltonian in Eq. (2), the current operator simply reads

$$\mathbf{j}(\mathbf{k}) = v_{\mathbf{k}}^{a} a_{\mathbf{k}}^{\dagger} a_{\mathbf{k}} + v_{\mathbf{k}}^{b} b_{\mathbf{k}}^{\dagger} b_{\mathbf{k}}, \tag{16}$$

where $v_{\mathbf{k}}^{a(b)} = \nabla \varepsilon_{\mathbf{k}}^{a(b)}$ with the dispersion energy $\varepsilon_{\mathbf{k}}^{a(b)}$ is defined in Eq. (3). Using the Bogoliubov transformation one can express the current operators in the new fermionic operators defined in Eqs. (7). Owing to the diagonal form of the Hamiltonian written in Eq. (11), we simply deliver an expression for the real part of the optical conductivity as

$$\sigma(\omega) = \frac{\pi}{\omega}\frac{1}{N}\sum_{\mathbf{k}} \eta_{\mathbf{k}}^2 \xi_{\mathbf{k}}^2 \left(v_{\mathbf{k}}^{a} - v_{\mathbf{k}}^{b}\right)^2 \left[n_F\left(E_{\mathbf{k}}^{a}\right) - n_F\left(E_{\mathbf{k}}^{b}\right)\right]$$
$$\times \left[\delta\left(\omega + E_{\mathbf{k}}^{a} - E_{\mathbf{k}}^{b}\right) - \delta\left(\omega - E_{\mathbf{k}}^{a} + E_{\mathbf{k}}^{b}\right)\right] \tag{17}$$

where the prefactors $\eta_{\mathbf{k}}$ and $\xi_{\mathbf{k}}$ have been defined in Eqs. (9) and the quasiparticle energies are given in Eq. (12). The real part of the optical conductivity in the excitonic system can be thus straightforwardly evaluated if the self-consistent solutions in the previous section are delivered.

B. Dynamical excitonic susceptibility function

Another quantity to analyze the dynamical excitonic excitations is the dynamical excitonic susceptibility function that might induce signatures of the excitonic fluctuations close to the critical points of the excitonic condensate transition. In the momentum space, the dynamical excitonic susceptibility function at a momentum $\mathbf{q}$ can be written as

$$\chi(\mathbf{q}, \omega) = -\frac{1}{N}\sum_{\mathbf{k}\mathbf{k}'} \langle\langle a_{\mathbf{k}}^{\dagger} b_{\mathbf{k}+\mathbf{q}} | b_{\mathbf{k}'+\mathbf{q}}^{\dagger} a_{\mathbf{k}'} \rangle\rangle_{\mathcal{H}}. \tag{18}$$

The two-particle correlation function in the summation might be evaluated by the equation of motion method, i.e., one arrives at

$$\omega \langle\langle a_{\mathbf{k}}^{\dagger} b_{\mathbf{k}+\mathbf{q}} | b_{\mathbf{k}'+\mathbf{q}}^{\dagger} a_{\mathbf{k}'} \rangle\rangle_{\mathcal{H}} = \langle [a_{\mathbf{k}}^{\dagger} b_{\mathbf{k}+\mathbf{q}}; b_{\mathbf{k}'+\mathbf{q}}^{\dagger} a_{\mathbf{k}'}] \rangle$$
$$+ \langle\langle [a_{\mathbf{k}}^{\dagger} b_{\mathbf{k}+\mathbf{q}}; \mathcal{H}] | b_{\mathbf{k}'+\mathbf{q}}^{\dagger} a_{\mathbf{k}'} \rangle\rangle_{\mathcal{H}}. \tag{19}$$

With the Hamiltonian $\mathcal{H}$ given in Eq. (2) the last term in Eq. (19) might appear the higher-order Green's functions. In the random phase approximation, the excess operators might be factorized and one finds

$$\sum_{\mathbf{k}''\mathbf{q}_1} \langle\langle a_{\mathbf{k}}^{\dagger} b_{\mathbf{k}''} a_{\mathbf{k}''-\mathbf{q}_1}^{\dagger} a_{\mathbf{k}+\mathbf{q}-\mathbf{q}_1} | b_{\mathbf{k}'+\mathbf{q}}^{\dagger} a_{\mathbf{k}'} \rangle\rangle_{\mathcal{H}}$$
$$\approx \sum_{\mathbf{q}_1} \langle n_{\mathbf{k}+\mathbf{q}-\mathbf{q}_1}^{a} \rangle \langle\langle a_{\mathbf{k}}^{\dagger} b_{\mathbf{k}+\mathbf{q}} | b_{\mathbf{k}'+\mathbf{q}}^{\dagger} a_{\mathbf{k}'} \rangle\rangle_{\mathcal{H}}$$
$$- \sum_{\mathbf{k}_2} \langle n_{\mathbf{k}}^{a} \rangle \langle\langle a_{\mathbf{k}_2}^{\dagger} b_{\mathbf{k}_2+\mathbf{q}} | b_{\mathbf{k}'+\mathbf{q}}^{\dagger} a_{\mathbf{k}'} \rangle\rangle_{\mathcal{H}}, \tag{20}$$

and

$$\sum_{\mathbf{k}''\mathbf{q}_1}\langle\langle b^\dagger_{\mathbf{k}+\mathbf{q}_1} b_{\mathbf{k}''} a^\dagger_{\mathbf{k}''-\mathbf{q}_1} b_{\mathbf{k}+\mathbf{q}} | b^\dagger_{\mathbf{k}'+\mathbf{q}} a_{\mathbf{k}'}\rangle\rangle_{\mathcal{H}}$$
$$\approx \sum_{\mathbf{q}_1}\langle n^b_{\mathbf{k}+\mathbf{q}_1}\rangle\langle\langle a^\dagger_{\mathbf{k}} b_{\mathbf{k}+\mathbf{q}} | b^\dagger_{\mathbf{k}'+\mathbf{q}} a_{\mathbf{k}'}\rangle\rangle_{\mathcal{H}}$$
$$- \sum_{\mathbf{k}_2}\langle n^b_{\mathbf{k}+\mathbf{q}}\rangle\langle\langle a^\dagger_{\mathbf{k}_2} b_{\mathbf{k}_2+\mathbf{q}} | b^\dagger_{\mathbf{k}'+\mathbf{q}} a_{\mathbf{k}'}\rangle\rangle_{\mathcal{H}}. \quad (21)$$

In the evaluations above, we have assumed that the system is in the normal state, all terms multiplying with the excitonic order parameters, therefore, are eliminated. In the normal state, $\delta = 0$, the Hamiltonian in Eq. (4) has been diagonalized, the expectation values in Eqs. (19)–(21) are simply determined and finally one delivers an expression of the dynamical excitonic susceptibility function in a popular form

$$\chi(\mathbf{q},\omega) = \frac{-\chi^0(\mathbf{q},\omega)}{1 + U\chi^0(\mathbf{q},\omega)}, \quad (22)$$

where

$$\chi^0(\mathbf{q},\omega) = \frac{1}{N}\sum_{\mathbf{k}} \frac{\langle n^b_{\mathbf{k}}\rangle - \langle n^a_{\mathbf{k}+\mathbf{q}}\rangle}{\omega + i0^+ - \bar{\varepsilon}^a_{\mathbf{k}+\mathbf{q}} + \bar{\varepsilon}^b_{\mathbf{k}}} \quad (23)$$

plays as the bare excitonic susceptibility function with the energies $\bar{\varepsilon}^{a(b)}_{\mathbf{k}}$ given in Eq. (3) and $\langle n^{a(b)}_{\mathbf{k}}\rangle = n_F(\bar{\varepsilon}^{a(b)}_{\mathbf{k}})$. Similar to the optical conductivity quantity in Eq. (17), the dynamical excitonic susceptibility function in Eq. (22) can be easily evaluated in case of the solution of the self-consistent equations is achieved.

IV. NUMERICAL RESULTS AND DISCUSSION

To analyze in detail the signatures of the dynamical properties of the excitonic condensation state in semimetallic and semiconductor materials, in this section, we address numerical results of the optical conductivity and dynamical excitonic susceptibility function evaluated analytically in Eqs. (17) and (22), respectively. In doing so, one has to find a solution of the self-consistent Eqs. (5), (6), and (13) for a set of parameters given in the Hamiltonian (1). In our numerical calculation, without generality, $t^a = 1$ is chosen as the unit of energy and $t^b = -0.3$ is fixed to illustrate the direct band-gap situation with the valence hole is usually more localized than the conduction electron. In this study, the chemical potential μ is adjusted to ensure the half-filled band case, i.e., $n^a + n^b = 1$.

First of all, we analyze the optical properties of the system in the ground state by discussing the real part of the optical conductivity spectra at zero temperature. The real part of the optical conductivity represents the optical absorption and provides information about the formation of excitons in the system. In Fig. 1, the real part of the zero-temperature optical conductivity $\sigma(\omega)$ is displayed for some values of the Coulomb interaction U at $\varepsilon^b = -2.0$. Note here that in our calculation, ε^b is specified in the case of $\varepsilon^a = 0$ is fixed. At a value of Coulomb interaction in which the system stabilizes in the excitonic condensation state, one always finds that the optical conductivity gets a sharp peak and then suddenly drops down to zero at a given energy ω_c by lowering frequency. For $\omega < \omega_c$, the optical conductivity $\sigma(\omega)$ is

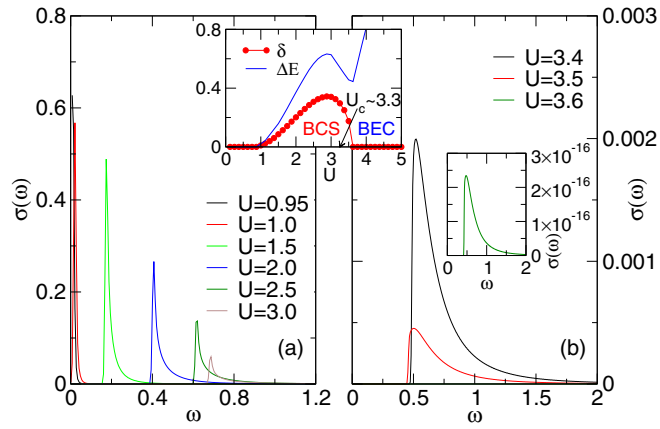

FIG. 1. The real part of the optical conductivity $\sigma(\omega)$ for different values of the Coulomb interaction U at $\varepsilon^b = -2$ and $T = 0$ in the semimetal (a) and semiconducting (b) situations. The larger inset shows the excitonic condensate order parameter δ and energy gap ΔE as functions of U. $U_c = 3.3$ indicates the critical Coulomb interaction of the BCS-BEC excitonic crossover. The smaller inset in the panel (b) plots $\sigma(\omega)$ for $U = 3.6$.

completely zero. Once U is small, the Coulomb interaction is not sufficiently large enough to establish the electron-hole bound state, the excitons are not formed and the system stabilizes in the electron-hole plasma state. The optical conductivity thus typifies the Drude behavior as found in the normal metal [see black-solid line in Fig. 1(a)]. Increasing the Coulomb interaction, the system stabilizes in the excitonic condensation state (see the red symbols in the inset). The excitonic condensate order parameter increases as increasing the Coulomb interaction, that is also indicated in the signature of the optical conductivity spectra in which ω_c increases in the order of 2δ. Due to the presence of the sufficiently large Coulomb interaction, electrons in the conduction band can bind together with the hole in the valence band and the hybridization between the bands develops corresponding to establishing the coherent state of excitons. That interorbital interaction is enough to yield the peak in the optical conductivity. However, at small U, the hybridization happens only in a narrow range around the Fermi level for a given ε^b and one finds the sharp peak in the optical conductivity spectrum. Increasing U, the hybridization is expanded with more electrons and holes carrying momenta deviating from the Fermi level contributing to the formation of the coherent state. Meanwhile, owing to the Hartree shift, increasing U also reinforces the separation between the conduction band and the valence band. The Fermi level thus becomes less important. The peak thus broadens and shifts to the higher energy and as increasing the interaction strength. In this situation, the system still settles in the semimetal state and the system typifies in the BCS-type of the excitonic condensation state [see Fig. 1(a)].

In the case with $U > U_c$ the system settles in the semiconducting state corresponding to the stability of the BEC excitonic condensate (U_c here is the critical value of the Coulomb interaction for the BCS-BEC crossover of the excitonic condensate, see the inset). In this case, the peak of optical conductivity strongly reduces and the spectrum is widely expanded for $\omega > \omega_c$. At $\omega < \omega_c$, the optical

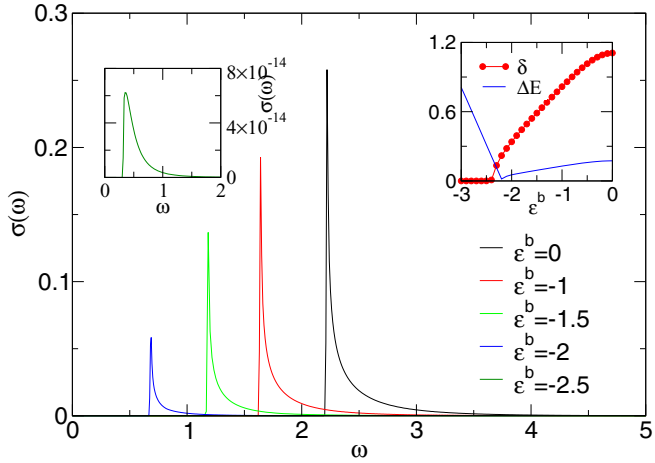

FIG. 2. The real part of the optical conductivity $\sigma(\omega)$ for different ε^b at zero temperature and $U = 3$. The left inset shows the optical conductivity spectrum at $\varepsilon^b = -2.5$ and the right inset plots the excitonic condensate order parameter δ and the energy gap ΔE as functions of ε^b.

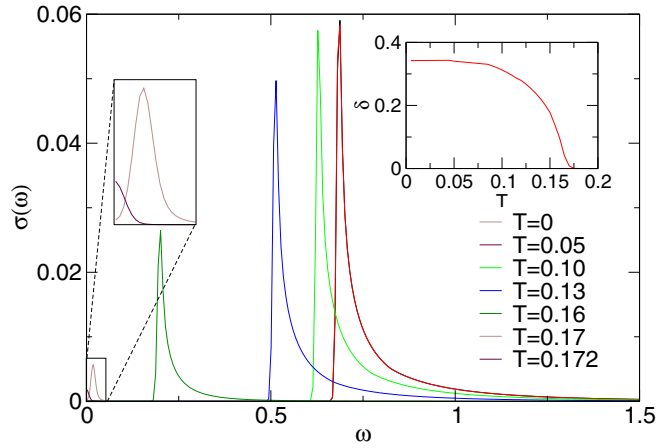

FIG. 3. The real part of the optical conductivity $\sigma(\omega)$ for different temperature T with $U = 3$ at $\varepsilon^b = -2.0$. The inset shows the excitonic condensate order parameter δ depending on temperature T for the set of parameters. Here we also zoom in to clear the signatures of $\sigma(\omega)$ for large temperatures $T = 0.17$ and $T = 0.172$.

conductivity signature also completely disappears. However, these signatures are significant and valid only in the excitonic condensation state with the spontaneous electron-hole hybridization. Out of the stability, i.e., in the normal semiconducting state, although one finds the disappearance, however, it is owing to the gap ΔE opening due to the Hartree shift that rapidly increases as increasing U (see the blue line in the inset). The ω_c thus becomes large, nevertheless, the height of the peak suddenly becomes uncountable [see blue line in Fig. 1(b)]. The optical conductivity spectra discussed above can be applicable to analyze the low-energy excitonic condensate features of semimetal Ta_2NiSe_5 or semiconductor Ta_2NiS_5 [6,7].

To address the external pressure affecting the optical properties of the excitonic condensation state in the system, we show in Fig. 2 the real part of the optical conductivity $\sigma(\omega)$ for various on-site valence electron energies ε^b at a given Coulomb coupling $U = 3$ and at zero temperature. Note that here we have fixed $\varepsilon^a = 0$, the on-site energy ε^b, therefore, represents the overlap between the noninteracting valence and conduction bands, indicating an effect of the external pressure on the semimetal-semiconducting transition systems [27,28]. Indeed, at $\varepsilon^b = 0$, one finds a robust overlap between two non-interacting conduction and valence bands corresponding to the strong external pressure applied to the system. In this case, the optical conductivity shows the sharp peak with high spectral weight and suddenly drops down at $\omega = \omega_c$. Lowering ε^b moves the valence band far from the conduction band with respect to reducing the external pressure and the peak in the optical conductivity shifts to the left with decreasing ω_c. The decrease of the spectral weight by lowering ε^b also indicates the depression of the electron-hole hybridization due to decreasing of the external pressure (see also the red symbols in the right inset). Especially, at very low ε^b, for instance at $\varepsilon^b = -2.5$, the two bands are completely separated, the system settles in the normal semiconducting state and the optical seemingly to be insignificant (see the left inset and blue line in the right inset in Fig. 2).

The stability of the excitonic condensate is further demonstrated by the temperature evolution of the optical conductivity. In Fig. 3 we address the real part of the optical conductivity $\sigma(\omega)$ for different temperatures T at given Coulomb coupling $U = 3$ and $\varepsilon^b = -2$. At low temperature, owing to the sufficient large Coulomb interaction the hybridization between the electrons in the conduction band and holes in the valence band might be formed and the excitonic condensation state is established. That is indicated by the sharp peak in the optical conductivity spectrum or the nonzero value of the excitonic order parameter δ. Increasing the temperature, the thermal fluctuations are reinforced, that eliminate the electron-hole pairing state. The peak of the optical conductivity spectrum, therefore, moves to the left with reducing its spectral weight. At large temperatures, all electron-hole pairs are destroyed and the system settles in the high-temperature electron-hole plasma state. The optical conductivity thus evaluates as the Drude form in the normal semimetal state (see the maroon-solid line in Fig. 3).

Above optical conductivity spectra have addressed the signatures of the optical absorption of excitons in the condensation state. The dynamical properties out of the order state thus still missing. In the rest of this section, we focus on discussing the excitonic fluctuations before the condensate becomes stabilized by analyzing signatures of the dynamical excitonic susceptibility function. Recent studies have released that the zero-momentum excitons become most favored in the forming of the excitonic condensation state in the semimetal Ta_2NiSe_5 [8,9,29,30]. In this paper, therefore, we would intently consider the dynamical excitonic susceptibility function at momentum $\mathbf{q} = \mathbf{0}$ to analyze the fluctuations of the excitonic condensation state.

In Fig. 4, we illustrate the imaginary part of the dynamical excitonic susceptibility function at the zero-momentum $\mathrm{Im}\chi(\omega) \equiv \mathrm{Im}\chi(\mathbf{q} = \mathbf{0}, \omega)$ evaluated in Eq. (22) for different Coulomb interactions U at $\varepsilon^b = -2$ and $T = 0.25$. In the range of the parameters, the excitonic condensate is probably out of the order and the dynamical excitonic susceptibility

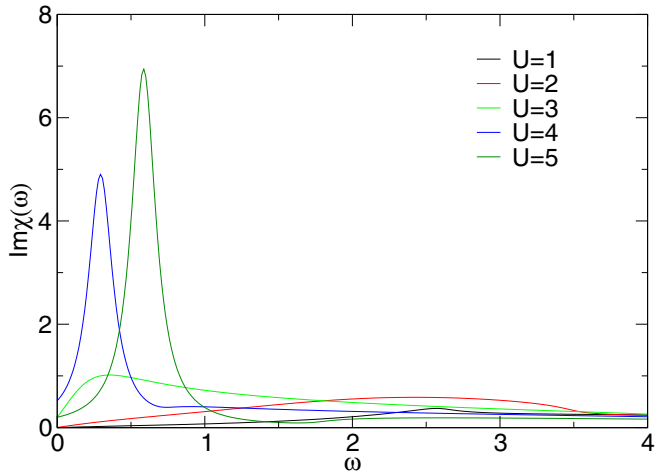

FIG. 4. The imaginary part of the dynamical excitonic susceptibility function for different values of the Coulomb interaction U at $\varepsilon^a = -2.0$ and $T = 0.25$.

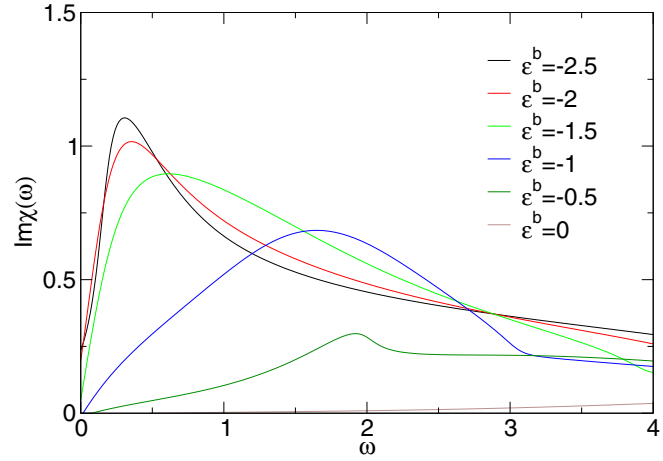

FIG. 5. The imaginary part of the dynamical excitonic susceptibility function for some values of the valence electron on-site energy ε^b at $U = 3$ and $T = 0.25$.

function would express the excitonic excitations before the condensed state becomes stabilized. For small Coulomb interaction $U \leqslant 3$, one finds a wide spreading of the dynamical susceptibility with low spectral weight. In this range of the Coulomb interaction, the system settles in a high-temperature semimetal state, the excitonic fluctuations thus seem to be insignificant, although, by increasing U the susceptibility function peak shifts to the lower frequency specifying that the bound excitonic coherence becomes more or less established. The bound of excitonic coherence becomes dramatically significant in the case of large Coulomb interaction, i.e., at $U \geqslant 4$. In this range, the system stabilizes in the high-temperature semiconducting state. The imaginary part of the dynamical excitonic susceptibility function shows a sharp peak at low frequency. The dramatic accretion of the peak signatures in the semiconducting state here specifies the extreme development of the bound excitonic coherence before the condensate transition and that corresponds to the formation of excitons out of the condensation state in the semiconducting side. This halo phase has been addressed in previous studies in the EFKM [16] or in the simple effective-mass Mott-Wannier-type model [4]. However, the coherence preformed excitons in the semiconducting state in the present study is the most significantly viewed in the signatures of the dynamical excitonic susceptibility function. Increasing U with respect to moving far from the boundary of the phase transition, the higher frequency-shifted peak in the susceptibility indicates the slacker bound coherence excitonic state. Note that the dynamical excitonic susceptibility functions addressed here are evaluated at the extremely large temperatures, the correlations in the systems thus become less important, which is synonymous with a weak-coupling situation [19]. The present results examined in the UHF approximation thus are reliable even for large Coulomb interaction [20–22].

The possibility of the appearance of the preformed excitons in the semiconducting side is also indicated in the signatures of the dynamical excitonic susceptibility function at a given mediated Coulomb coupling but with small external pressure. Indeed, Fig. 5 shows us that the imaginary part of $\chi(\omega)$ gets a sharp peak at a small frequency in the case of $\varepsilon^b = -2.5$. In that situation, the system settles into a semiconducting state (see Fig. 2). Increasing the external pressure corresponding to increasing the valence electron on-site energy ε^b, the system sustains in the semimetal state, the peak thus moves to the right with depressing the spectral weight. Especially, for $\varepsilon^b = 0$, the signature of the $\mathrm{Im}\chi(\omega)$ releases the property of the nearly free high-temperature electron-hole plasma system.

Lastly, we analyze the impact of the thermal fluctuations on the bound excitonic coherence state above the excitonic condensate transition points by considering the temperature dependence of the dynamical excitonic susceptibility function. Figure 6 addresses the imaginary part of the susceptibility for some different temperatures at a given Coulomb coupling for fixed $\varepsilon^b = -2$. At mediated Coulomb interaction, $U = 3$ for instance, Fig. 6(a) shows us that at a given temperature, the dynamical susceptibility function gets a single peak. Lowering temperature shifts the peak to the left and reinforces the spectral weight. That signature indicates the tendency of the bound excitonic coherent state might appear once the temperature reaches the critical points. The thermal

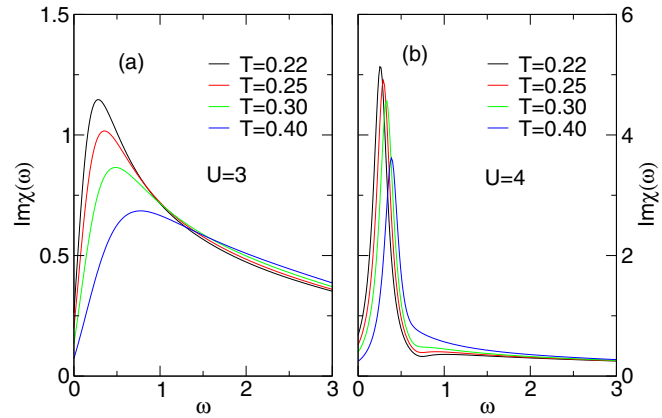

FIG. 6. The imaginary part of the dynamical excitonic susceptibility function for different values of the temperature T at $U = 3$ (a) and $U = 4$ (b) with $\varepsilon^b = -2$.

fluctuations thus play an important role, that might destroy the coherence of the excitons in case of sufficiently large temperature. However, the signature of the excitonic coherence only becomes significant once the system settles in the semiconducting side. Indeed, at large Coulomb interaction, Fig. 6(b) displays a sharp resonance peak at a low frequency of the dynamical excitonic susceptibility function. The spectral weight is much larger than that observed in the case of mediated Coulomb coupling with respect to the semimetal state [c.f Fig. 6(a)]. Signature of the $\mathrm{Im}\chi(\omega)$ in Fig. 6(b) thus expresses the stability of the bound excitonic coherent state above the transition points. The preformed excitons thus have been specified in the high-temperature semiconducting state. The impress of the thermal fluctuations once again appears in this situation releasing that increasing the temperature has pressed down the bound electron-hole pair coherence.

V. CONCLUSIONS

To conclude, we have addressed the low-energy dynamical properties of the excitonic condensation state in semimetal and semiconducting materials by analyzing the optical conductivity and dynamical excitonic susceptibility functions. By using the unrestricted Hartree-Fock approximation for the extended Falicov-Kimball model we have derived a set of self-consistent equations, so the quasiparticle energies can be numerically evaluated. This helps us inspect the stability of the excitonic condensation state in signatures of the excitonic order parameters and the optical conductivity in the Kubo formula. In the framework of the random phase approximation, the dynamical excitonic susceptibility function for the model is also discussed. Our numerical results release in detail the low-frequency dynamical properties of the bound coherence excitonic state both inside and outside of the excitonic condensation state. Indeed, inside the excitonic condensation state, the optical conductivity shows a sharp peak at a frequency that is twice as of the excitonic condensate order parameter. The peak becomes less significant if the system is out of the excitonic condensate. In the meanwhile, the dynamical excitonic susceptibility function presents the signatures of the excitonic fluctuations above the transition points. In the semimetal side with sufficiently large Coulomb interaction, one finds a dominant peak at low frequency in the dynamical excitonic susceptibility spectra, indicating the possibility of the resonance bound excitonic condensate. The signature is dramatically reinforced inside of the semiconducting state with large Coulomb interaction. In this case, the dynamical susceptibility exhibits an extremely high peak at low energy and that specifies the stability of the bound excitonic condensation state of the preformed excitons in the semiconducting materials. Contributions of the quantum fluctuations beyond the present approximations in considering the low-energy excitonic condensation properties would be worthwhile for future studies.

ACKNOWLEDGMENT

This research is funded by Ministry of Education and Training, Vietnam, under Grant No. B2021-MDA-14.

[1] N. F. Mott, Philos. Mag. **6**, 287 (1961).
[2] R. Knox, in *Solid State Physics*, edited by F. Seitz and D. Turnbull (Academic Press, New York, 1963), Suppl. 5 p. 100.
[3] W. Kohn, in *Many Body Physics*, edited by C. de Witt and R. Balian (Gordon & Breach, New York, 1968).
[4] F. X. Bronold and H. Fehske, Phys. Rev. B **74**, 165107 (2006).
[5] D. Ihle, M. Pfafferott, E. Burovski, F. X. Bronold, and H. Fehske, Phys. Rev. B **78**, 193103 (2008).
[6] K. Sugimoto, S. Nishimoto, T. Kaneko, and Y. Ohta, Phys. Rev. Lett. **120**, 247602 (2018).
[7] J. Lee, C.-J. Kang, M. J. Eom, J. S. Kim, B. I. Min, and H. W. Yeom, Phys. Rev. B **99**, 075408 (2019).
[8] P. A. Volkov, M. Ye, H. Lohani, I. Feldman, A. Kanigel, and G. Blumberg, npj Quantum Mater. **6**, 52 (2021).
[9] K. Kim, H. Kim, J. Kim, C. Kwon, J. S. Kim, and B. J. Kim, Nat. Commun. **12**, 1969 (2021).
[10] Q.-H. Ninh and V.-N. Phan, Phys. Status Solidi B **258**, 2000564 (2021).
[11] D. Geffroy, J. Kaufmann, A. Hariki, P. Gunacker, A. Hausoel, and J. Kuneš, Phys. Rev. Lett. **122**, 127601 (2019).
[12] A. Niyazi, D. Geffroy, and J. Kuneš, Phys. Rev. B **102**, 085159 (2020).
[13] V.-N. Phan, K. W. Becker, and H. Fehske, Phys. Rev. B **81**, 205117 (2010).
[14] K. Seki, R. Eder, and Y. Ohta, Phys. Rev. B **84**, 245106 (2011).
[15] B. Zenker, D. Ihle, F. X. Bronold, and H. Fehske, Phys. Rev. B **83**, 235123 (2011).
[16] N. V. Phan, H. Fehske, and K. W. Becker, Europhys. Lett. **95**, 17006 (2011).
[17] B. Bucher, P. Steiner, and P. Wachter, Phys. Rev. Lett. **67**, 2717 (1991).
[18] P. Wachter, B. Bucher, and J. Malar, Phys. Rev. B **69**, 094502 (2004).
[19] S. Chakrabarty and Z. Nussinov, Phys. Rev. B **84**, 064124 (2011).
[20] A. Georges, G. Kotliar, W. Krauth, and M. J. Rozenberg, Rev. Mod. Phys. **68**, 13 (1996).
[21] U. Gupta and A. K. Rajagopal, Phys. Rev. A **21**, 2064 (1980).
[22] S. Hong and G. D. Mahan, Phys. Rev. B **50**, 7284 (1994).
[23] L. M. Falicov and J. C. Kimball, Phys. Rev. Lett. **22**, 997 (1969).
[24] J. Hubbard, Proc. R. Soc. London A **276**, 238 (1963).
[25] B. Zenker, H. Fehske, and C. D. Batista, Phys. Rev. B **82**, 165110 (2010).
[26] H. Bruus and K. Flensberg, *Many-Body Quantum Theory in Condensed Matter Physics: An Introduction* (Oxford University Press, New York, 2004).
[27] P. Wachter, Adv. Mater. Phys. Chem. **08**, 120 (2018).
[28] P. Wachter and B. Bucher, Phys. B: Condens. Matter **408**, 51 (2013).
[29] Y.-S. Zhang, J. A. N. Bruin, Y. Matsumoto, M. Isobe, and H. Takagi, Phys. Rev. B **104**, L121201 (2021).
[30] T.-H.-H. Do and V.-N. Phan, J. Phys.: Condens. Matter **34**, 165602 (2022).